

Article

Porous Hybrid Materials Based on Mesotetrakis(Hydroxyphenyl) Porphyrins and TiO₂ for Efficient Visible-Light-Driven Hydrogen Production

Li-Yuan Huang, Jian-Feng Huang *, Yang Lei, Su Qin and Jun-Min Liu *

MOE Laboratory of Bioinorganic and Synthetic Chemistry, Lehn Institute of Functional Materials, School of Chemistry, and School of Materials Science and Engineering, Sun Yat-sen University, Guangzhou 510275, China; hlyuan@mail2.sysu.edu.cn (L.-Y.H.); leiy56@mail2.sysu.edu.cn (Y.L.); qins3@mail2.sysu.edu.cn (S.Q.)

* Correspondence: huangjf39@mail.sysu.edu.cn (J.-F.H.); liujunm@mail.sysu.edu.cn (J.-M.L.); Tel.: +86-020-8411-5178 (J.-F.H. & J.-M.L.)

Received: 7 May 2020; Accepted: 7 June 2020; Published: 11 June 2020



Abstract: A series of highly robust nano-micro hybrid materials based on meso-tetra(4-hydroxyphenyl) porphyrins (M = H, Pd, Zn) and titanium dioxide (denoted as THPP-TiO₂, THPP-Pd-TiO₂, and THPP-Zn-TiO₂) have been prepared by a facile sol-gel method for the first time. When Pt nanoparticles are incorporated in these hybrids, Pt/THPP-Pd-TiO₂ achieves good H₂ production activity (2025.4 μmol g⁻¹ h⁻¹ and 12.03 μmol m⁻² h⁻¹), higher than that of Pt/THPP-Zn-TiO₂ (1239.8 μmol g⁻¹ h⁻¹ and 7.46 μmol m⁻² h⁻¹) and Pt/THPP-TiO₂ (576.8 μmol g⁻¹ h⁻¹ and 4.02 μmol m⁻² h⁻¹), owing to the different central metal ions in porphyrins. The best activity of Pt/THPP-Pd-TiO₂ would be attributed to the two-center catalysis from coordination Pd metal ions and Pt nanoparticles, while the higher activity of Pt/THPP-Zn-TiO₂ than Pt/THPP-TiO₂ could be ascribed to the more effective light harvesting and electron transfer between THPP-Zn and TiO₂. In addition, the hybridized Pt/THPP-Pd-TiO₂ catalyst exhibits unattenuated hydrogen production stability even after recycling the experiment 10 times (cumulative turnover number of 5111 after 50 h), far superior to that of the surface-sensitized Pt/THPP-Pd/TiO₂ catalyst with analogous components, due to the more stable Ti-O bonds between four phenols in porphyrins and TiO₂ for the hybrid system. The present study provides a promising approach for constructing stable organic-inorganic hybrid systems with unique hierarchical structures for efficient light absorption and electron transfer.

Keywords: porphyrin photosensitizer; titanium dioxide; organic-inorganic hybrid material; photocatalytic H₂ evolution; durability

1. Introduction

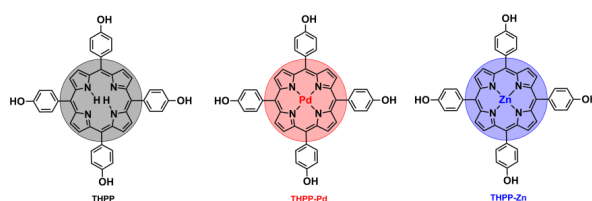
Photocatalytic hydrogen generation over the semiconductor-based photocatalyst under solar light irradiation is a promising approach to solving current energy and environmental issues [1–4]. The active and stable photocatalysts are vital for highly efficient hydrogen production. As a good candidate photocatalyst, TiO₂ has been widely used owing to its low toxicity, abundance and stability against the light irradiation [5–10]. The photoactivity of TiO₂ is closely relevant to particle size, crystal form, surface morphology, and pore structure, and therefore the proper engineering of TiO₂ in photocatalytic system can greatly improve its activity. TiO₂ with a large surface area and micro/mesoporous structures can facilitate reactant/product transfer and enhance optical absorption efficiency, which shows a perfect performance in dye-sensitized TiO₂ photocatalysis [11–13]. However, pure TiO₂ has poor

response to visible light due to its wide band gap and fast electron-hole recombination, which limit its photocatalytic activity. In general, noble metal (Au, Ag, and Pt) is usually loaded on TiO₂, which can effectively inhibit fast charge carrier recombination [14].

To enhance the light response of the TiO₂-based photocatalytic systems, the two most efficient strategies, bandgap engineering (cation/anion doping, or semiconductor heterojunction construction, etc.) [15–18] and dye sensitization [11–13], have been proposed. In this regard, sensitizing TiO₂ with photosensitizer is a facile but effective way to realize the visible-light-driven photocatalysis of TiO₂. Among all the reported dye sensitizers, metal complexes and metal-free organic dyes are widely applied in TiO₂-based photocatalytic hydrogen evolution [11]. Porphyrins and their metallic derivatives with conjugate structures have attracted much attention due to their excellent light absorption, prospective photoexcitation, electron-transfer ability, low cost and excellent thermal and chemical stability [19,20]. Moreover, their photoelectronic properties can be easily tuned by introducing diverse functional groups on the peripheries or metal ions on the centers of their macrocycles. Thus, porphyrins are promising candidates for constructing functional nanomaterials. R. Banerjee et al. reported the synthesis of a porphyrin-based porous polymer and its application in sensitizing TiO₂ nanoparticles by ball-milling method, and the obtained composite showed higher activity for H₂ evolution than the parent precursor under visible light irradiation [21]. Liu et al. reported photocatalytic systems with Sn-porphyrins as the sensitizer by surface sensitization, and the H₂ evolution activities of a series of Sn-porphyrins with different functional groups and Pt nanoparticles with different surface stabilizers were investigated [22]. Nevertheless, the common dye-sensitized TiO₂ photocatalytic systems are still unsatisfactory because the dye would shed from the semiconductor and follow by photodegradation [23]. Moreover, charge injection from dye to TiO₂ is an inefficient process, which limits the efficiency of photogenerated charges [24,25]. Due to insufficient adsorption stability and low charge mobility, it is necessary to anchor the dyes onto TiO₂ by a covalent bond for exploring durable and efficient photosynthesis systems.

Recently, organic/inorganic hybrid materials have been proven as very promising in obtaining new materials with desirable properties because the combined advantageous characteristics of organic and inorganic parts can realize the optimization and complementarity of their properties [26–31]. To prepare TiO₂-based nano hybrid materials, many approaches, such as dispersion polymerization [32], hydrothermal method [33], template-assisted growth [34], and sol-gel method [35–37] have been developed, among which the sol-gel is a facile method for preparing multi-component and highly dispersive materials.

Herein, with meso-tetra(4-hydroxyphenyl) porphyrins (M = H, Pd, Zn, denoted as THPP, THPP-Pd and THPP-Zn) (Scheme 1) as visible-light absorption antennas, respectively, a series of novel TiO₂-based organic/inorganic hybrid nanocomposites (denoted as THPP-TiO₂, THPP-Pd-TiO₂, and THPP-Zn-TiO₂) were fabricated using four firm Ti-O bonds as the interfacial linkers by a simple sol-gel method. When Pt nanoparticles (Pt NPs) were loaded onto the hybrids, these hybrid systems could display stable photocatalytic H₂ evolution properties under visible light irradiation, showing an increasing trend in the sequence of Pt/THPP-Pd-TiO₂ > Pt/THPP-Zn-TiO₂ > Pt/THPP-TiO₂ due to the effect of central metal ions in porphyrins. Compared with analogous surface-sensitized Pt/THPP-Pd/TiO₂ catalyst, the photocatalytic stability of the hybridized Pt/THPP-Pd-TiO₂ was significantly improved. In addition, the mechanism of electron transfer and photocatalytic H₂ production in the hybrid materials was investigated.



Scheme 1. Molecular structures of THPP, THPP-Pd and THPP-Zn.

2. Results and Discussion

The synthesis of the three porphyrins, THPP-TiO₂, THPP-Pd-TiO₂, THPP-Zn-TiO₂ and their materials loaded with Pt NPs, and comparative Pt/THPP-Pd/TiO₂ was included in the experimental section. The X-ray diffraction (XRD) patterns of the samples are shown in Figure 1. Five diffraction peaks at 25.53°, 38.12°, 48.22°, 54.18°, and 62.94° of Gel-TiO₂, THPP-TiO₂, THPP-Pd-TiO₂ and THPP-Zn-TiO₂ samples corresponded to (101), (103), (200), (105), and (204) planes of the crystalline anatase structure of titanium dioxide. The diffraction peaks of THPP-TiO₂, THPP-Pd-TiO₂, and THPP-Zn-TiO₂ matched well to those of pure Gel-TiO₂, indicating that the presence of porphyrins in the hybrid did not change the crystallinity of TiO₂. The relatively regular diffraction peaks without the peaks of other impurities showed the high purity of these samples.

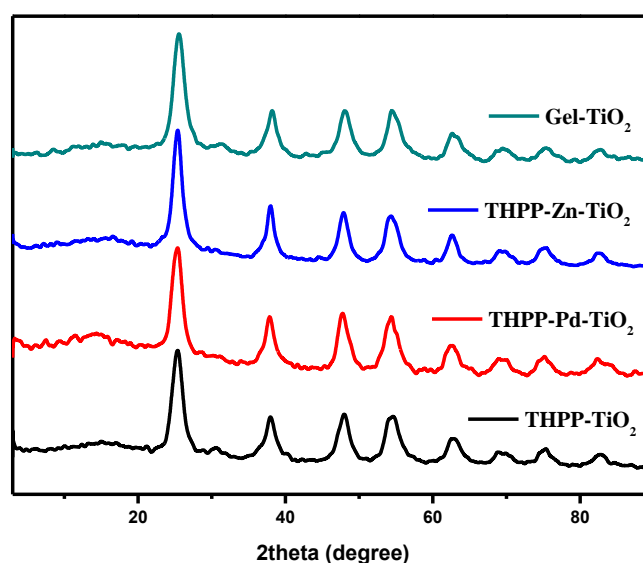


Figure 1. The XRD patterns of Gel-TiO₂, THPP-TiO₂, THPP-Pd-TiO₂ and THPP-Zn-TiO₂.

The surface areas of the photocatalyst play an important role in the hydrogen production in the photocatalytic system. Nitrogen adsorption–desorption isotherms were measured at 77 K to obtain the Brunauer–Emmett–Teller (BET) surface areas and pore size distributions of the samples (Figures S1 and S2 and Table S1). The BET surface areas of THPP-TiO₂, THPP-Pd-TiO₂, THPP-Zn-TiO₂, Gel-TiO₂, and, for comparison, P25-TiO₂ were evaluated to be 143.4, 166.1, 168.3, 162.9, and 55.4 m² g^{−1}, respectively. The results suggested that the sol-gel method could increase the BET surface areas of TiO₂. In addition, the micro/mesoporous structure, comprising both micropores (1~2 nm) and mesopores (3~5 nm), could be observed in porphyrin-TiO₂ and Gel-TiO₂ materials, in contrast to that (29 nm) of mesoporous P25-TiO₂, which shortened the transport length and contributed to the faster diffusion of the electrons from the bulk to the surface, thus inhibiting the charge recombination and increasing the catalytic efficiency.

The morphologies of the as-prepared samples have been observed by the scanning electron microscopy (SEM) and transmission electron microscopy (TEM). The SEM image in Figure 2A reveals that the porphyrin-TiO₂ presented a random aggregation of sheets which were closely associated with each other. The SEM elemental mapping of THPP-TiO₂, THPP-Pd-TiO₂, THPP-Zn-TiO₂, indicated that the elements C and N for THPP-TiO₂, C, N, and Pd for THPP-Pd-TiO₂, and C, N, and Zn for THPP-Zn-TiO₂ dispersed homogeneously throughout the whole hybrid material, respectively (Figure 2B–D).

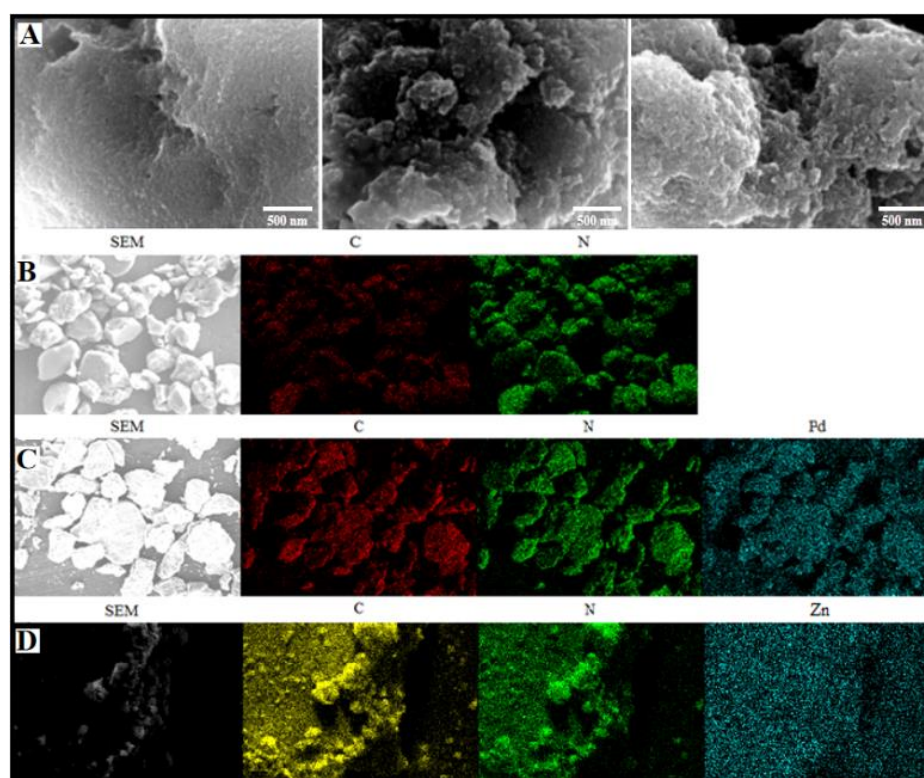


Figure 2. (A) TEM of THPP-TiO₂, THPP-Pd-TiO₂, and THPP-Zn-TiO₂, and the elemental mappings image of (B) THPP-TiO₂, (C) THPP-Pd-TiO₂ and (D) THPP-Zn-TiO₂.

The TEM image of the porphyrin-TiO₂ samples (Figure 3A–C) showed that the hybrid materials were composed of nanospheres with an average diameter of 10 nm. The lattice fringe spacing was estimated to be 0.357 nm, in accordance with the (101) plane of anatase TiO₂ (Figure 3D–F). The selected area electron diffraction (SAED) results of the porphyrin-TiO₂ samples confirmed the formation of the anatase phase in TiO₂ (Figure 3G–I).

UV-vis absorption spectra of three porphyrins in DMF solution and in solid-state, Gel-TiO₂, and the hybrid materials based on porphyrins and TiO₂ are shown in Figure 4. All the porphyrins exhibited strong absorption in the visible region, ranging from 400 to 700 nm. The peak centered at about 420 nm was ascribed to the Soret absorption band originating from the $a_{1u}(\pi) \rightarrow e_g(\pi)$ transition (S0–S2), while the absorption bands ranging from 500 to 700 nm were attributed to the weaker Q bands of $a_{2u}(\pi) \rightarrow e_g(\pi)$ transitions (S0–S1). The absorption intensities of the three porphyrins were measured to be close to the values reported in the literature [38]. Compared with THPP, the absorption peak numbers of THPP-Pd and THPP-Zn in the region above 500 nm were reduced from 4 to 2, owing to the increased porphyrin ring symmetry after coordination with metal, which reduced the degree of molecular orbital splitting and improved the degeneracy. Although the maximum absorption wavelengths (λ_{max}) of the Soret absorption bands were similar, the Q-band absorption wavelengths increased in the order of THPP-Pd < THPP < THPP-Zn. Particularly, THPP-Zn had the highest extinction coefficient and most obvious red-shift among those porphyrins, because it was easier for ZnPyd to occur the metal-to-ligand charge transfer (MLCT) owing to the weaker interaction between Zn²⁺ (3d₁₀) and Py macrocycle ion without any single electron [39]. This better absorption and charge transfer properties in relation to Zn²⁺ ions were favorable for the H₂ production reaction.

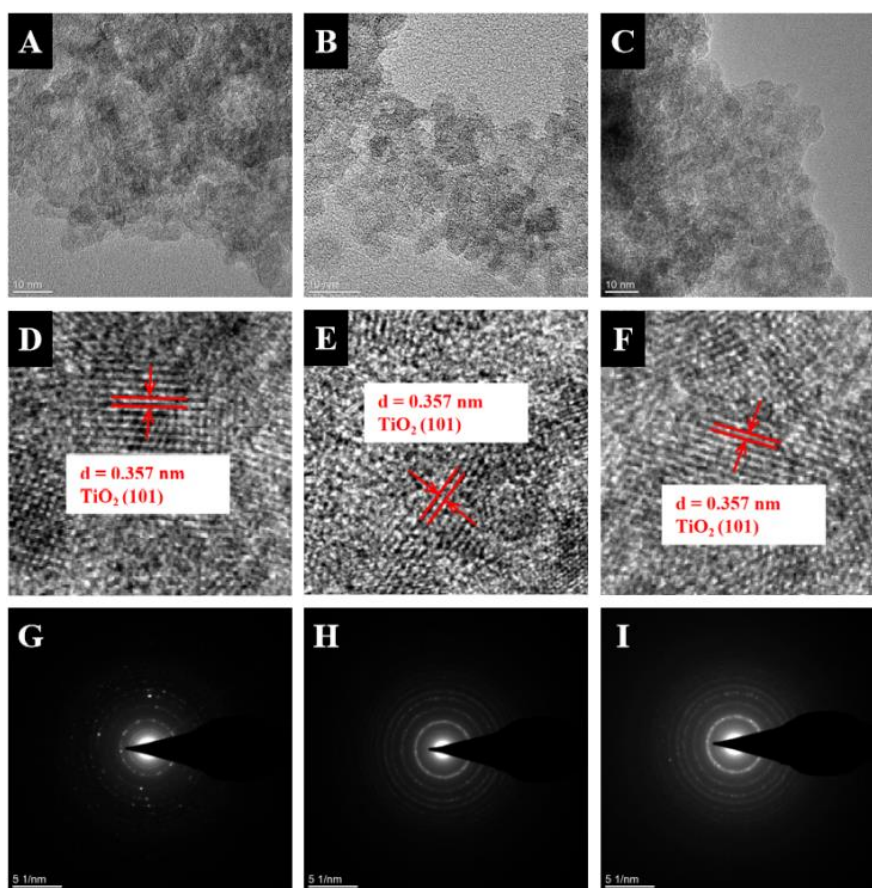


Figure 3. TEM of (A) THPP-TiO₂, (B) THPP-Pd-TiO₂ and (C) THPP-Zn-TiO₂; HRTEM of (D) THPP-TiO₂, (E) THPP-Pd-TiO₂ and (F) THPP-Zn-TiO₂, and SAED of (G) THPP-TiO₂, (H) THPP-Pd-TiO₂ and (I) THPP-Zn-TiO₂.

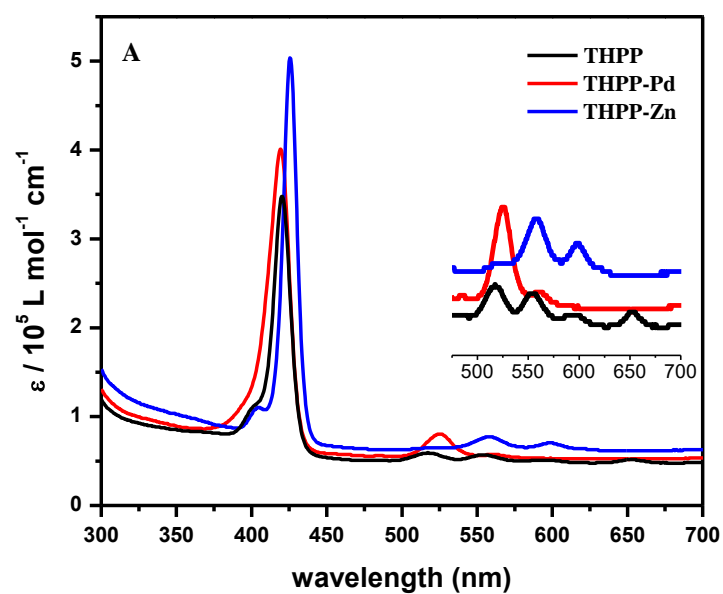


Figure 4. Cont.

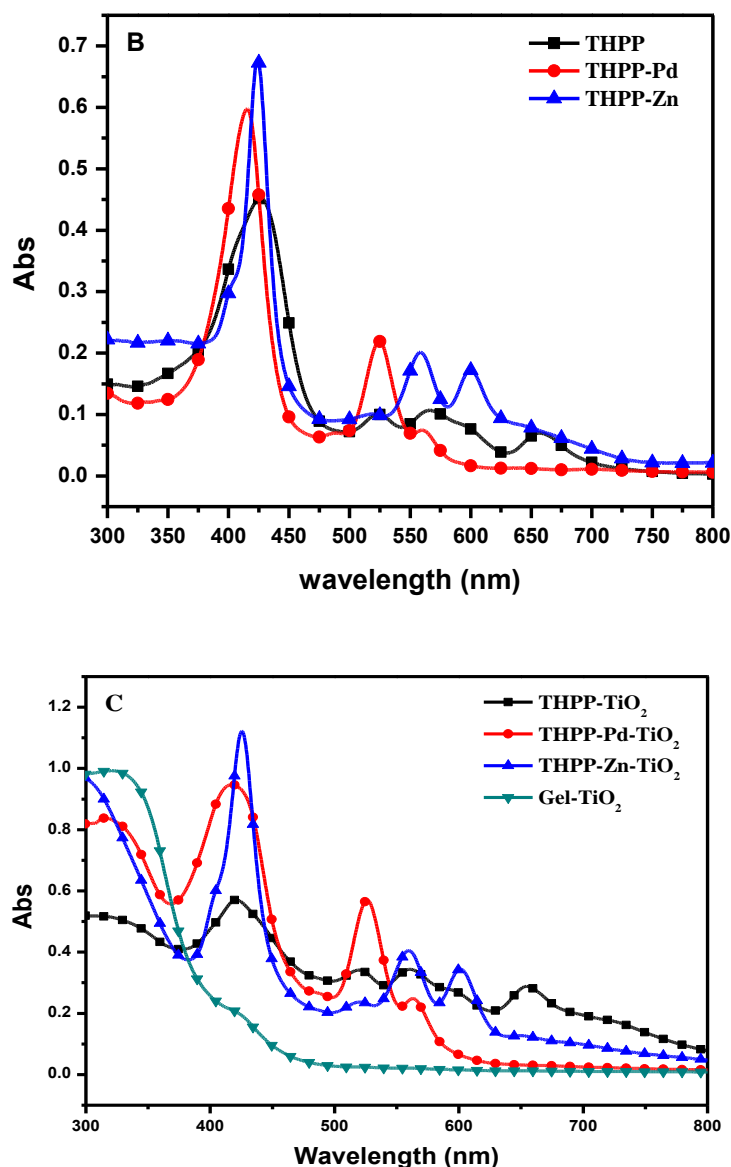


Figure 4. UV-vis absorption spectra of THPP, THPP-Pd, and THPP-Zn (A) in DMF solution and (B) in solid-state, and (C) UV-vis solid-state diffraction spectra of THPP-TiO₂, THPP-Pd-TiO₂, THPP-Zn-TiO₂ and Gel-TiO₂.

When the porphyrins was doped into TiO₂ by the sol-gel method, the hybrids exhibited a red-shift and significantly extended the absorption profile, which most probably originated from the strong interaction between the –OH moieties of porphyrins and –Ti atoms of the TiO₂, in agreement with our previous work [40]. For the Gel-TiO₂, a strong absorption peak at 325 nm with an absorption edge of 450 nm corresponded to a 3.25 eV band gap. In contrast to Gel-TiO₂ with a single optical band gap in Tauc plots (Figure S3), the hybrid materials based on porphyrins and TiO₂ showed multiple band gaps. These narrow band gaps (2.6–2.8 eV) could be caused by the doping of the porphyrins, while the wide band gap of 3.0–3.3 eV for the three porphyrin-based hybrids should come from the inorganic component TiO₂, respectively.

To prove the feasibility of conducting photocatalytic H₂ production, the first oxidation potentials of THPP, THPP-Pd, and THPP-Zn were measured by cyclic voltammograms (CVs) to obtain HOMO value (1.12, 1.08, and 1.10 V vs. NHE) (Figure S4 and Table S2). The zero-zero excitation energies were estimated from the intersection of the absorption and emission spectra as 1.90, 2.19, and 2.05 eV for THPP, THPP-Pd, and THPP-Zn, respectively (Figure S5 and Table S2). The LUMO levels of THPP,

THPP-Pd, and THPP-Zn (-0.78 , -1.11 , and -0.95 V vs. NHE) were calculated from the HOMO values of the porphyrins and the zero-zero excitation energies. The valence-band potential of Gel-TiO₂ was reported to be -0.5 V vs. NHE in our previous literature [41], which was more positive than the LUMO values of the three porphyrins and more negative than the redox potential of H⁺/H₂, and thus facilitated electron injection from the porphyrins to TiO₂ and favoured the proton reduction to realize photocatalytic H₂ generation. Among the three porphyrins, the higher LUMO level of THPP-Pd than those of THPP and THPP-Zn implied that there is a stronger driving force to promote electron transfer from THPP-Pd to TiO₂, which could accelerate the rate of hydrogen production. On the other hand, the first oxidation potentials of the porphyrins were more positive than that of the redox couple (0.84 ± 0.12 V vs. NHE) of triethanolamine as a sacrificial agent [42], beneficial to promoting dye regeneration and suppressing the recombination between the injected electrons and the dye cation radical (Figure 5).

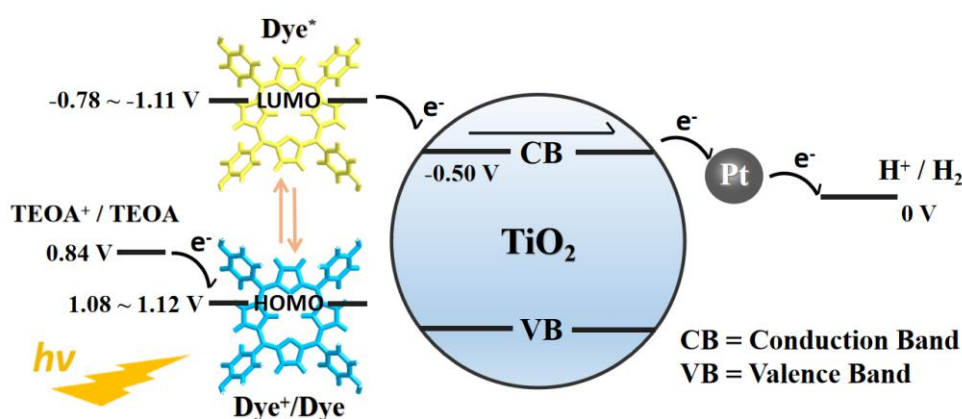


Figure 5. Proposed mechanism of photocatalytic H₂ production over Pt/porphyrin-TiO₂.

For evaluating the influence of coordination metal ions on the photoactivity of the as-prepared materials, the photocatalytic experiments were performed in the visible light region with the Pt/THPP-TiO₂, Pt/THPP-Pd-TiO₂ and Pt/THPP-Zn-TiO₂ catalysts using 0.5 wt% Pt particles as co-catalyst and TEOA as sacrificial electron donor. Figure 6 illustrated the H₂ evolution plots of these hybrid systems and the corresponding data were summarized in Table S3. Pt/THPP-Pd-TiO₂ catalyst exhibited higher hydrogen production activity ($2025.4 \mu\text{mol g}^{-1} \text{h}^{-1}$ based on the catalyst mass and $12.03 \mu\text{mol m}^{-2} \text{h}^{-1}$ based on the surface area) than those of Pt/THPP-Zn-TiO₂ ($1239.8 \mu\text{mol g}^{-1} \text{h}^{-1}$ and $7.46 \mu\text{mol m}^{-2} \text{h}^{-1}$) and Pt/THPP-TiO₂ ($576.8 \mu\text{mol g}^{-1} \text{h}^{-1}$ and $4.02 \mu\text{mol m}^{-2} \text{h}^{-1}$). The result indicated that coordinated Pd metal ions play an essential role in the photoactivity of Pt/THPP-Pd-TiO₂. For the known photochemical molecular devices (PMDs), the NⁿN-chelated N_nMX₂ (M = Pd²⁺, Pt²⁺ or Rh²⁺, X = Cl⁻, Br⁻ or I⁻, n = 2 or 4) coordination polyhedron was commonly employed as a catalyst centre, in which the dissociation of the terminal X⁻ anions during the photocatalytic process was found [43,44]. It was also reported that Pd(Py)₄ motifs possessing a PdN₄ environment with four monodentate pyridyl ligands could be used as the catalytic centres for photocatalytic H₂ evolution, where the breaking of the Pd-N bond and the formation of hydride intermediate may happen [45,46]. Thus, we deduced that the higher amount of H₂ exhibited by the Pt/THPP-Pd-TiO₂ hybrid may be attributed to the two-center catalysis from coordination Pd metal ions of porphyrin dye and Pt nanoparticles. In addition, the better catalytic activity of Pt/THPP-Zn-TiO₂ than Pt/THPP-TiO₂ could be attributed to the more effective light harvesting and charge transfer between THPP-Zn and TiO₂ mentioned above. The apparent quantum yields (AQYs) of corresponding samples were measured and followed the order of Pt/THPP-Pd-TiO₂ > Pt/THPP-Zn-TiO₂ > Pt/THPP-TiO₂ (Table S4), in consistence with the results of their photocatalytic H₂ production.

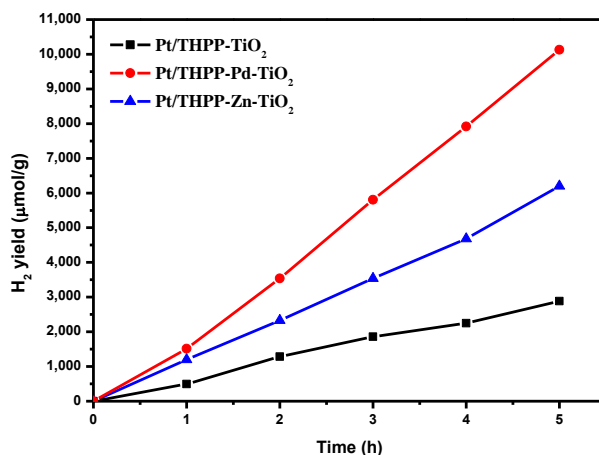


Figure 6. H₂ production curves of Pt/THPP-TiO₂, Pt/THPP-Pd-TiO₂, and Pt/THPP-Zn-TiO₂ in an aqueous solution of 10% TEOA under visible-light irradiation ($\lambda > 420$ nm).

In order to confirm the efficiencies of the photocatalysts and their stability under UV light irradiation, control experiments of the three catalysts under complete UV-vis irradiation have been performed (Figure S6) and all catalysts exhibited higher H₂ production activities than those under visible light, owing to the effective UV-responses of the porphyrins and TiO₂ substrate. It was noteworthy that Pt/THPP-Zn-TiO₂ showed the highest activity under complete UV-vis irradiation. This result could be ascribed to the better absorption of THPP-Zn compared to THPP-Pd and THPP in the UV band, which could be observed in the UV-vis absorption spectra of THPP, THPP-Pd, and THPP-Zn (Figure 4).

To check the contribution of the Pd coordination metal ions to H₂ production, the control experiments with THPP-TiO₂, THPP-Pd-TiO₂ and THPP-Zn-TiO₂ without Pt NPs for photocatalysis have been performed (Figure 7 and Table S3). It was found that the H₂ generation rate of THPP-Pd-TiO₂ without Pt NPs was 230.1 $\mu\text{mol g}^{-1} \text{h}^{-1}$ (1.37 $\mu\text{mol m}^{-2} \text{h}^{-1}$), while no obvious amount of H₂ was detected for THPP-TiO₂ and THPP-Zn-TiO₂. These results supported that Pd coordination metal ions were conducive to the photocatalytic H₂ evolution activity of THPP-Pd-TiO₂.

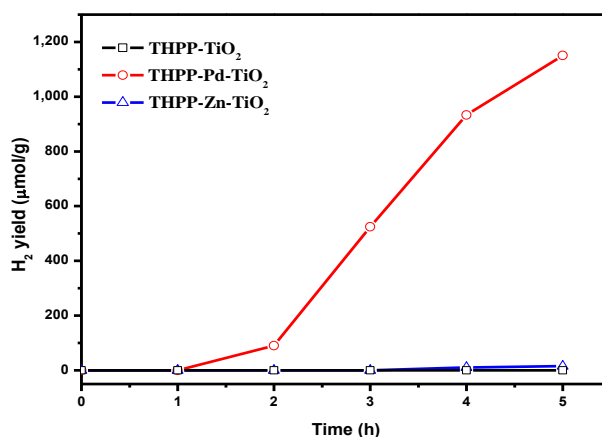


Figure 7. H₂ production curves of THPP-TiO₂, THPP-Pd-TiO₂, and THPP-Zn-TiO₂ in an aqueous solution of 10% TEOA under visible-light irradiation ($\lambda > 420$ nm).

To study the difference of catalytic activity of the hybrid system Pt/THPP-Pd-TiO₂ and the surface sensitization system Pt/THPP-Pd/TiO₂, the control experiments of two catalysts were carried out (Figure 8 and Table S5). In the initial 5 h light irradiation, two catalysts with 0.5 wt% Pt loading and approximate porphyrin amounts exhibited the same H₂ evolution activity. However, in second and third run, H₂-production activity of hybrid Pt/THPP-Pd-TiO₂ were rising from initial 2025.4 to

2755.9 $\mu\text{mol g}^{-1} \text{h}^{-1}$ (12.03 to 16.38 $\mu\text{mol m}^{-2} \text{h}^{-1}$) in contrast with the continuous decline in the activity of surface sensitization Pt/THPP-Pd/TiO₂ to 1110.3 $\mu\text{mol g}^{-1} \text{h}^{-1}$ (6.81 $\mu\text{mol m}^{-2} \text{h}^{-1}$) after the third run. During the photocatalytic reaction process, the THPP-Pd dye seriously detached from the Pt/THPP-Pd/TiO₂ material under visible light irradiation, but the detaching phenomena were not contributed to the Pt/THPP-Pd-TiO₂ catalysts even after they were used for 10 times and recycled. As shown in Figure 9 and Table S5, the Pt/THPP-Pd-TiO₂ catalyst showed an outstanding stability without a decrease in photocatalysis. The TON_{H₂} calculated as the number of moles of H₂ divided by the number of moles of Pt was 5111 after 50 h, indicating the higher photocatalytic activity and stability of the hybrid materials than those of the common surface dye-sensitized system. The inorganic component TiO₂ in the hybrid materials was expected to be able to protect the THPP-Pd, and the stable linkages between THPP-Pd and TiO₂ were beneficial for efficient electron transfer from THPP-Pd* to TiO₂. Thus, organic–inorganic components in the hybrid system, in other words, have a synergistic effect on the photocatalytic reaction.

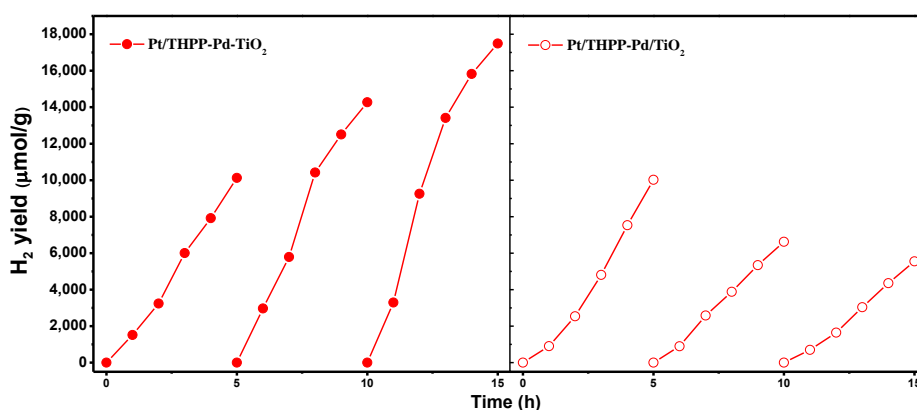


Figure 8. Time courses of H₂ production over Pt/THPP-Pd-TiO₂ and Pt/THPP-Pd/TiO₂ under $\lambda > 420$ nm light irradiation.

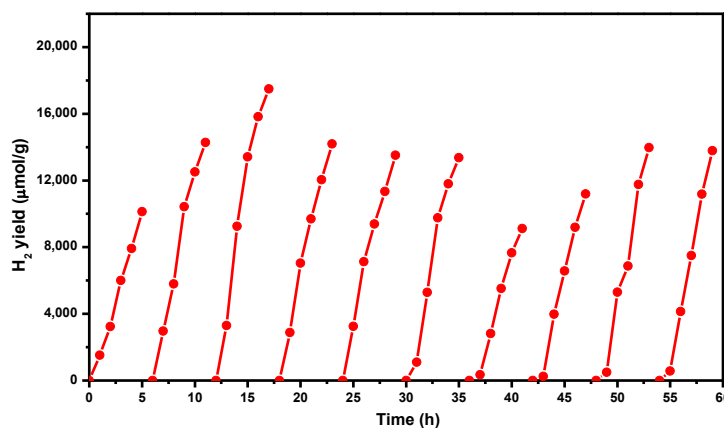


Figure 9. Photocatalytic H₂ production against the recyclability of Pt/THPP-Pd-TiO₂ under visible light irradiation ($\lambda > 420$ nm) in 100 mL H₂O/TEOA (9: 1 v/v).

3. Conclusions

In summary, we have, for the first time, developed a series of unique hierarchical hybrid materials (THPP-TiO₂, THPP-Pd-TiO₂, and THPP-Zn-TiO₂) by combining TiO₂ and porphyrins through a sol-gel method, which possessed a highly accessible surface area as well as delivered excellent charge separation and transport efficiency due to the stable Ti–O linkage, resulting in efficient and persistent photocatalytic water splitting activities when loaded with Pt nanoparticles. The absorption spectra, electrochemical properties and charge transfer processes of those porphyrins were investigated to

vary along with the central metal ions. The effects of central metal ions led to the catalytic properties of the hybrids for H₂ production indicating a rising trend in the sequence of Pt/THPP-Pd-TiO₂ > Pt/THPP-Zn-TiO₂ > Pt/THPP-TiO₂. Especially, Pt/THPP-Pd-TiO₂ showed the best H₂ production activity (2025.4 μmol g⁻¹ h⁻¹ and 12.03 μmol m⁻² h⁻¹) among the three hybrids under visible light irradiation owing to two catalytic centers from coordination Pd metal ions of porphyrin dye and Pt nanoparticles. The superior activity of Pt/THPP-Zn-TiO₂ to Pt/THPP-TiO₂ could be attributed to the more effective optical absorption of THPP-Zn and electron transfer between THPP-Zn and TiO₂. Comparatively, the hybrid Pt/THPP-Pd-TiO₂ exhibited superior stability to the analogous surface dye-sensitized Pt/THPP-Pd/TiO₂ system under similar photocatalytic conditions and an impressive TON of 5111 has been achieved through a ten-cycle photoreaction without a decrease for 50 h. The present results reveal that varying the central metal ions in porphyrins or conducting interface and microstructure modulation is a facile strategy to optimize the photogenerated charge transfer pathway and utilize the visible light of sunlight to significantly enhance the efficiency of the solar-to hydrogen conversion efficiency.

Supplementary Materials: The following are available online at <http://www.mdpi.com/2073-4344/10/6/656/s1>, Figure S1: N₂ adsorption-desorption isotherms of Gel-TiO₂, THPP-TiO₂, THPP-Pd-TiO₂ and THPP-Zn-TiO₂ at 77 K, Figure S2: The pore size distributions of A) THPP-TiO₂, B) THPP-Pd-TiO₂ and C) THPP-Zn-TiO₂, Table S1: BET surface areas, pore volumes and pore widths of Gel-TiO₂, THPP-TiO₂, THPP-Pd-TiO₂ and THPP-Zn-TiO₂ derived from 77 K N₂ sorption isotherms, Figure S3: Tauc plots of THPP-TiO₂, THPP-Pd-TiO₂, THPP-Zn-TiO₂ and Gel-TiO₂, Figure S4: Cyclic voltammogram of THPP, THPP-Pd and THPP-Zn in 0.1 M TBAPF₆ THF solution with a scan rate of 40 mV s⁻¹, Figure S5: Absorption and emission spectra of A) THPP, B) THPP-Pd, and C) THPP-Zn measured in THF solution, Table S2: The energy levels and electrochemical data of THPP, THPP-Pd and THPP-Zn, Table S3: H₂ production data and calculated TON values of hybrid catalysts of THPP, THPP-Pd and THPP-Zn with or without Pt NPs under visible light in 5 h, Table S4: AQY results for H₂ production of Pt/THPP-TiO₂, Pt/THPP-Pd-TiO₂ and Pt/THPP-Zn-TiO₂ catalysts (6 mg for each sample) after 0.5 h irradiation under 425 nm LED light source, Figure S6: H₂ production curves of Pt/THPP-TiO₂, Pt/THPP-Pd-TiO₂, and Pt/THPP-Zn-TiO₂ in an aqueous solution of 10% TEOA under complete UV-vis irradiation, Table S5: H₂ production data and calculated TON values of Pt/THPP-Pd-TiO₂ and Pt/THPP-Pd/TiO₂ in cyclic photocatalytic experiment.

Author Contributions: J.-M.L. designed the research and wrote the paper. J.-F.H. directed the experiments and helped in paper preparation. L.-Y.H. carried out most of the syntheses and measurements. Y.L. and S.Q. helped in experiments and data analyses. All authors discussed the results and commented on the manuscript. All authors have read and agreed to the published version of the manuscript.

Funding: This research was funded by the National Natural Science Foundation Project of China (grant no. 21572280, 21975291, and 61772053), the NSF of Guangdong Province (grant no. 2019A1515011640), Science and Technology Plan Project of Guangzhou (grant no. 201707010114), and the FRF for the Central Universities (grant no. 19lgpy12).

Conflicts of Interest: The authors declare no conflict of interest.

References

1. Chen, S.; Takata, T.; Domen, K. Particulate photocatalysts for overall water splitting. *Nat. Rev. Mater.* **2017**, *2*, 17050. [[CrossRef](#)]
2. Wang, Z.; Li, C.; Domen, K. Recent developments in heterogeneous photocatalysts for solar-driven overall water splitting. *Chem. Soc. Rev.* **2019**, *48*, 2109–2125. [[CrossRef](#)] [[PubMed](#)]
3. Tilley, S.D. Recent advances and emerging trends in photo-electrochemical solar energy conversion. *Adv. Energy Mater.* **2019**, *9*, 1802877. [[CrossRef](#)]
4. Qi, J.; Zhang, W.; Cao, R. Solar-to-hydrogen energy conversion based on water splitting. *Adv. Energy Mater.* **2018**, *8*, 1701620. [[CrossRef](#)]
5. Chen, X.; Li, C.; Grätzel, M.; Kostecki, R.; Mao, S.S. Nanomaterials for renewable energy production and storage. *Chem. Soc. Rev.* **2012**, *41*, 7909–7937. [[CrossRef](#)]
6. Nakata, K.; Fujishima, A. TiO₂ photocatalysis: Design and applications. *J. Photochem. Photobiol. C* **2012**, *13*, 169–189. [[CrossRef](#)]
7. Kubacka, A.; Fernández-García, M.; Colón, G. Advanced nanoarchitectures for solar photocatalytic applications. *Chem. Rev.* **2012**, *112*, 1555–1614. [[CrossRef](#)] [[PubMed](#)]

8. Kudo, A.; Miseki, Y. Heterogeneous photocatalyst materials for water splitting. *Chem. Soc. Rev.* **2009**, *38*, 253–278. [[CrossRef](#)]
9. Miyoshi, A.; Nishioka, S.; Maeda, K. Water splitting on rutile TiO₂-based photocatalysts. *Chem. Eur. J.* **2018**, *24*, 18204–18219. [[CrossRef](#)]
10. Lee, C.-Y.; Zou, J.; Bullock, J.; Wallace, G.G. Emerging approach in semiconductor photocatalysis: Towards 3D architectures for efficient solar fuels generation in semi-artificial photosynthetic systems. *J. Photochem. Photobiol. C* **2019**, *39*, 142–160. [[CrossRef](#)]
11. Cecconi, B.; Manfredi, N.; Montini, T.; Fornasiero, P.; Abboto, A. Dye-sensitized solar hydrogen production: The emerging role of metal-free organic sensitizers. *Eur. J. Org. Chem.* **2016**, *31*, 5194–5215. [[CrossRef](#)]
12. Ho, P.-Y.; Wang, Y.; Yiu, S.-C.; Yu, W.-H.; Ho, C.-L.; Huang, S. Starburst triarylamine donor-based metal-free photosensitizers for photocatalytic hydrogen production from water. *Org. Lett.* **2017**, *5*, 1048–1051. [[CrossRef](#)] [[PubMed](#)]
13. Tiwari, A.; Duvva, N.; Rao, V.N.; Venkatakrishnan, S.M.; Giribabu, L.; Pal, U. Tetrathiafulvalene scaffold-based sensitizer on hierarchical porous TiO₂: Efficient light-harvesting material for hydrogen production. *J. Phys. Chem. C* **2019**, *123*, 70–81. [[CrossRef](#)]
14. Su, R.; Tiruvalam, R.; Logsdail, A.J.; He, Q.; Downing, C.A.; Jensen, M.T.; Dimitratos, N.; Kesavan, L.; Wells, P.P.; Bechstein, R.; et al. Designer titania-supported Au-Pd nanoparticles for efficient photocatalytic hydrogen production. *ACS Nano* **2014**, *8*, 3490–3497. [[CrossRef](#)] [[PubMed](#)]
15. Ma, Y.; Wang, X.; Jia, Y.; Chen, X.; Han, H.; Li, C. Titanium dioxide-based nanomaterials for photocatalytic fuel generations. *Chem. Rev.* **2014**, *114*, 9987–10043. [[CrossRef](#)]
16. Fang, W.; Xing, M.; Zhang, J. Modifications on reduced titanium dioxide photocatalysts: A review. *J. Photochem. Photobiol. C* **2017**, *32*, 21–39. [[CrossRef](#)]
17. Navarro, R.M.; Alvarez-Galvan, M.C.; Villoria de la Mano, J.A.; Al-Zahrani, S.M.; Fierro, J.L.G. A framework for visible-light water splitting. *Energy Environ. Sci.* **2010**, *3*, 1865–1882. [[CrossRef](#)]
18. Chen, X.; Shen, S.; Guo, L.; Mao, S.S. Semiconductor-based photocatalytic hydrogen generation. *Chem. Rev.* **2010**, *110*, 6503–6570. [[CrossRef](#)]
19. Urbani, M.; Grätzel, M.; Nazeeruddin, M.K.; Torres, T. Meso-substituted porphyrins for dye-sensitized solar cells. *Chem. Rev.* **2014**, *114*, 12330–12396. [[CrossRef](#)]
20. Song, H.; Liu, Q.; Xie, Y. Porphyrin-sensitized solar cells: Systematic molecular optimization, coadsorption and cosensitization. *Chem. Commun.* **2018**, *54*, 1811–1824. [[CrossRef](#)]
21. Mukherjee, G.; Thote, J.; Aiyappa, H.B.; Kandambeth, S.; Banerjee, S.; Vanka, K.; Banerjee, R. A porous porphyrin organic polymer (PPOP) for visible light triggered hydrogen production. *Chem. Commun.* **2017**, *53*, 4461–4464. [[CrossRef](#)] [[PubMed](#)]
22. Kuposova, E.; Liu, X.; Pendin, A.A.; Thiele, B.; Shumilova, G.; Ermolenko, Y.; Offenhäusser, A.; Mourzina, Y. Influence of Meso-substitution of the Porphyrin ring on enhanced hydrogen evolution in a photochemical system. *J. Phys. Chem. C* **2016**, *120*, 13873–13890. [[CrossRef](#)]
23. Huang, J.-F.; Lei, Y.; Xiao, L.-M.; Chen, X.-L.; Zhong, Y.-H.; Qin, S.; Liu, J.-M. Photocatalysts for H₂ generation from starburst triphenylamine/carbazole donor-based metal-free dyes and porous anatase TiO₂ cube. *ChemSusChem* **2020**, *13*, 1037–1043. [[CrossRef](#)] [[PubMed](#)]
24. Wang, Y.; Hong, J.; Zhang, W.; Xu, R. Carbon nitride nanosheets for photocatalytic hydrogen evolution: Remarkably enhanced activity by dye sensitization. *Catal. Sci. Technol.* **2013**, *3*, 1703–1711. [[CrossRef](#)]
25. Min, S.X.; Lu, G.X. Dye-sensitized reduced graphene oxide photocatalysts for highly efficient visible-light-driven water reduction. *J. Phys. Chem. C* **2011**, *115*, 13938–13945. [[CrossRef](#)]
26. Chen, Q.; Marco, N.D.; Yang, Y.; Song, T.-B.; Chen, C.-C.; Zhao, H.; Hong, Z.; Zhou, H.; Yang, Y. Under the spotlight: The organic-inorganic hybrid halide perovskite for optoelectronic applications. *Nano Today* **2015**, *10*, 355–396. [[CrossRef](#)]
27. Pan, Z.; Yao, L.; Zhai, J.; Yao, X.; Chen, H. Interfacial coupling effect in organic/inorganic nanocomposites with high energy density. *Adv. Mater.* **2018**, *30*, 1705662.
28. Chen, Y.; Shi, J. Chemistry of mesoporous organosilica in nanotechnology: Molecularly organic-inorganic hybridization into frameworks. *Adv. Mater.* **2016**, *28*, 3235–3272. [[CrossRef](#)]
29. Gobbi, M.; Orgiu, E.; Samorì, P. When 2D materials meet molecules: Opportunities and challenges of hybrid organic/inorganic van der Waals heterostructures. *Adv. Mater.* **2018**, *30*, 1706103. [[CrossRef](#)]

30. Lazzara, G.; Cavallaro, G.; Panchal, A.; Fakhrullin, R.; Stavitskaya, A.; Vinokurov, V.; Lvov, Y. An assembly of organic-inorganic composites using halloysite clay nanotubes. *Curr. Opin. Colloid Interface Sci.* **2018**, *35*, 42–50. [[CrossRef](#)]
31. Kaushik, A.; Kumar, R.; Arya, S.K.; Nair, M.; Malhotra, B.D.; Bhansali, S. Organic-inorganic hybrid nanocomposite-based gas sensors for environmental monitoring. *Chem. Rev.* **2015**, *115*, 4571–4606. [[CrossRef](#)] [[PubMed](#)]
32. Matsuyama, K.; Mishima, K. Preparation of poly(methyl methacrylate)-TiO₂ nanoparticle composites by pseudo-dispersion polymerization of methyl methacrylate in supercritical CO₂. *J. Supercrit. Fluids* **2009**, *49*, 256–264. [[CrossRef](#)]
33. Liu, N.; Chen, X.; Zhang, J.; Schwank, J.W. A review on TiO₂-based nanotubes synthesized via hydrothermal method: Formation mechanism, structure modification, and photocatalytic applications. *Catal. Today* **2014**, *225*, 34–51. [[CrossRef](#)]
34. Bhat, T.S.; Mali, S.S.; Korade, S.D.; Shaikh, J.S.; Karanjkar, M.M.; Hong, C.K.; Kim, J.H.; Patil, P.S. Mesoporous architecture of TiO₂ microspheres via controlled template assisted route and their photoelectrochemical properties. *J. Mater. Sci. Mater. El.* **2017**, *28*, 304–316. [[CrossRef](#)]
35. Macwan, D.P.; Dave, P.N.; Chaturvedi, S. A review on nano-TiO₂ sol-gel type syntheses and its applications. *J. Mater. Sci.* **2011**, *46*, 3669–3686. [[CrossRef](#)]
36. Akpan, U.G.; Hameed, B.H. The advancements in sol-gel method of doped-TiO₂ photocatalysts. *Appl. Catal. A* **2010**, *375*, 1–11. [[CrossRef](#)]
37. Zhang, K.; Wang, X.; Guo, X.; Dai, J.; Xiang, J. Fast sol-gel method to prepare mesoporous TiO₂ with high photocatalytic activity. *Nano* **2015**, *10*, 1550001. [[CrossRef](#)]
38. Wang, J.; Liu, D.; Liu, Q.; Peng, T.; Li, R.; Zhou, S. Effects of the central metal ions on the photosensitization of metalloporphyrins over carbon nitride for visible-light-responsive H₂ production. *Appl. Surf. Sci.* **2019**, *464*, 255–261. [[CrossRef](#)]
39. Liao, M.-S.; Scheiner, S. Electronic structure and bonding in metal porphyrins, metal = Fe, Co, Ni, Cu, Zn. *J. Chem. Phys.* **2002**, *117*, 205–219. [[CrossRef](#)]
40. Chen, Y.-F.; Huang, J.-F.; Shen, M.-H.; Liu, J.-M.; Huang, L.-B.; Zhong, Y.-H.; Qin, S.; Guo, J.; Su, C.-Y. A porous hybrid material based on calixarene dye and TiO₂ demonstrating high and stable photocatalytic performance. *J. Mater. Chem. A* **2019**, *7*, 19852–19861. [[CrossRef](#)]
41. Zhong, Y.-H.; Lei, Y.; Huang, J.-F.; Xiao, L.-M.; Chen, X.-L.; Luo, T.; Qin, S.; Guo, J.; Liu, J.-M. Design of an alkaline pyridyl acceptor-based calix[4]arene dye and synthesis of stable calixarene-TiO₂ porous hybrid materials for efficient photocatalysis. *J. Mater. Chem. A* **2020**, *8*, 8883–8891. [[CrossRef](#)]
42. Sun, H.; Hoffman, M.Z. Reductive quenching of the excited states of ruthenium(II) complexes containing 2,2'-bipyridine, 2,2'-bipyrazine and 2,2'-bipyrimidine ligands. *J. Phys. Chem. A* **1994**, *98*, 11719–11726. [[CrossRef](#)]
43. Pfeffer, M.G.; Schäfer, B.; Smolentsev, G.; Uhlig, J.; Nazarenko, E.; Guthmüller, J.; Kuhnt, C.; Wächter, M.; Dietzek, B.; Sundström, V.; et al. Palladium versus platinum: The metal in the catalytic center of a molecular photocatalyst determines the mechanism of the hydrogen production with visible light. *Angew. Chem. Int. Ed.* **2015**, *54*, 5044–5048. [[CrossRef](#)]
44. Tschierlei, S.; Presselt, M.; Kuhnt, C.; Yartsev, A.; Pascher, T.; Sundström, V.; Karnahl, M.; Schwalbe, M.; Schäfer, B.; Rau, S.; et al. Photophysics of an intramolecular hydrogen-evolving Ru-Pd photocatalyst. *Chem. Eur. J.* **2009**, *15*, 7678–7688. [[CrossRef](#)]
45. Dempsey, J.L.; Brunschwig, B.S.; Winkler, J.R.; Gray, H.B. Hydrogen evolution catalyzed by cobaloximes. *Acc. Chem. Res.* **2009**, *42*, 1995–2004. [[CrossRef](#)]
46. Manbeck, G.F.; Brewer, K.J. Photoinitiated electron collection in polyazine chromophores coupled to water reduction catalysts for solar H₂ production. *Coord. Chem. Rev.* **2013**, *257*, 1660–1675. [[CrossRef](#)]

